Astronomy & Astrophysics

Photodesorption and physical properties of CO ice as a function of temperature

G. M. Muñoz Caro[1], Y.-J. Chen[2], S. Aparicio[3], A. Jiménez-Escobar[1,4], A. Rosu-Finsen[5],
J. Lasne[5,6], and M. R. S. McCoustra[5]

[1] Centro de Astrobiología (CSIC-INTA), Ctra. de Ajalvir, km 4, Torrejón de Ardoz, 28850 Madrid, Spain
  e-mail: munozcg@cab.inta-csic.es
[2] Department of Physics, National Central University, Jhongli District, Taoyuan City 32054, Taiwan
[3] Instituto de Tecnologías Físicas y de la Información, Leonardo Torres Quevedo, ITEFI (CSIC), c/ Serrano 144, 28006 Madrid, Spain
[4] INAF−Osservatorio Astronomico di Palermo, P.za Parlamento 1, 90134 Palermo, Italy
[5] Institute of Chemical Sciences, School of Engineering and Physical Sciences, William Perkin Building G.19/G.28, Heriot-Watt University, Riccarton, EH14 4AS, Edinburgh, UK
[6] Laboratoire Interuniversitaire des Systèmes Atmosphériques (LISA), CNRS UMR 7583, Université Paris-Est Créteil, Université Paris Diderot, Faculté des Sciences et Technologie, 61 avenue du Général de Gaulle, 94010 Créteil Cedex, France

Received 13 January 2016 / Accepted 24 February 2016

ABSTRACT

Context. Ice photodesorption has been the topic of recent studies that aim to interpret the abundances of gas-phase molecules, in particular CO, toward cold interstellar regions. But little is known about the effect of the ice's physical properties on the photodesorption rate. The linear decrease observed in the photodesorption rate, as a function of increasing CO ice deposition temperature, was provisionally attributed to a more compact CO ice structure.
Aims. The goal of this work is to monitor the physical properties of solid CO as a function of ice deposition temperature. Then, we evaluate the possible link between the structure of ice and the ice's photodesorption rate.
Methods. Infrared spectroscopy is an efficient tool to monitor the structural evolution of pure ices during warm-up or irradiation. The infrared absorption bands of molecular ice components observed toward various space environments allow for the detection of H_2O, CO, CO_2, CH_3OH, NH_3, etc. Typically, a pure ice that is composed of one of these species displays significant changes in their mid-infrared band profiles as a result of warm-up. But, at most, only very subtle changes appear in the narrow CO ice infrared absorption band as the result of warm-up. We, therefore, also used vacuum-ultraviolet spectroscopy of CO ice to monitor the effect of temperature in the physical properties of the ice. Finally, temperature-programmed desorption and photo-desorption experiments for different CO ice deposition temperatures were performed.
Results. Mid-infrared and vacuum-ultraviolet spectroscopy showed that warm-up of CO ice that is deposited at 8 K did not lead to structural changes. Only CO ice samples deposited at temperatures above 20 K displayed different spectroscopic properties compared to lower deposition temperatures. The observed gradual and linear drop in the photodesorption rate of CO ice, as a function of increasing ice deposition temperature in the 7 to 20 K range, is, therefore, not due to a gradual re-structuring toward a more compact and crystalline ice, which is only triggered above 20 K and increases for higher deposition temperatures.
Conclusions. We suggest that this decrease of the photodesorption rate is related to the disorder of CO dipole molecules within the amorphous or glassy state, which influences the necessary transfer of photon energy from the first excited molecule to the desorbing molecule on the ice surface. The photodesorption yield of CO deposited at 20 K is about four times lower than at 7 K. Dust models should adopt CO photodesorption yields that are compatible with the thermal history of the cloud.

Key words. astrochemistry – ISM: lines and bands – ultraviolet: ISM – methods: laboratory: solid state – ISM: molecules – techniques: spectroscopic

1. Introduction

After H_2O, carbon monoxide (CO) is commonly the most abundant molecular component in interstellar and circumstellar icy grain mantles. The CO molecule is also the second most abundant, after H_2, in the gas phase of the interstellar medium. The CO gas abundances observed toward cold regions suggest that a non-thermal desorption mechanism is active. Therefore, numerous experimental studies were devoted to the infrared spectroscopy of CO ice, the structural changes in solid CO as a function of temperature or irradiation (Sandford & Allamandola 1988; Sandford et al. 1988; Kouchi 1990; Palumbo & Strazzulla 1993; Gerakines et al. 1996; Collings et al. 2004; Loeffler et al. 2005; Bisschop et al. 2006; Dartois 2006; Palumbo et al. 2006; Acharyya et al. 2007; etc.), and the search for a non-thermal desorption mechanism of pure CO ice, such as photodesorption (Öberg et al. 2007, 2009; Muñoz Caro et al. 2010; Fayolle et al. 2011; Chen et al. 2014; Cruz-Diaz et al. 2014).

Compared to that of other molecules, the photodesorption of CO has thus been studied in detail experimentally and using theoretical models (e.g., van Hemert et al. 2015). The CO photodesorption rate values that have been reported by Muñoz Caro et al. (2010) and Chen et al. (2014), respectively at 15 K and 14 K deposition temperatures, using a F-type microwave-discharged hydrogen UV lamp with comparable spectral emission, were 3.5×10^{-2} and 8.9×10^{-2} molecules per incident photon. If the factor 2.55 difference in their estimations of the total UV flux at the sample position, respectively 2.5×10^{14}, measured using actinometry, and 9.8×10^{13} photons cm^{-2} s^{-1}, measured with a

calibrated Ni-mesh, is taken into account, both works converge exactly to the same value of the photodesorption rate. The exception being for Lyman-α photons which, due to their very low absorption cross section in CO ice (Cruz-Diaz et al. 2014), other monochromatic photon energies also led to photodesorption rate values in the 10^{-2} range (Fayolle et al. 2011). We note that only the UV photons absorbed in the top 5 ± 1 ice monolayers participate in the photodesorption of CO (Muñoz Caro et al. 2010; Fayolle et al. 2011; Chen et al. 2014). The presence of H_2O or other molecules in the ice, like N_2, has an impact on the photodesorption yield of CO (Bertin et al. 2012, 2013). In pure CO_2 ice irradiation experiments, where CO is a photoproduct, a UV fluence, which is similar to that experienced by ice mantles during the quiescent molecular cloud lifetime, only led to ~4% photodesorption of the CO molecules formed (Martín-Doménech et al. 2015). Photodesorption rate values per incident photon, as reported by Fayolle et al. (2011) for different photon energies, were converted to rates in molecules that desorb per absorbed photon in the ice, leading to values near unity or higher (Cruz-Diaz et al. 2014). A linear decrease in the photodesorption rate as a function of ice deposition temperature in the 15 to 27 K range was reported by Öberg et al. (2007). These authors proposed that this effect is probably due to ice restructuring into a more compact configuration and noted that the observed linearity might be coincidental.

Most works reported in astrophysical journals characterize the solid CO samples using IR spectroscopy, which allows a comparison of laboratory data to observations of CO in icy grain mantles. Kouchi (1990) followed the evaporation of CO ice using mass spectrometry for the evolved gas and electron diffraction to monitor solid CO. It was found that the CO that was deposited at 10 K as amorphous ice becomes crystalline at 23 ± 1 K.

In this work, we extend the estimation of the photodesorption yields of CO (Öberg et al. 2009) to lower ice deposition temperatures, in the 7 to 20 K range. In addition, we use IR and vacuum-UV (VUV) spectroscopy to monitor the physical properties of CO ice during warm-up, or comparing the spectra of CO deposited at various temperatures. Compared to electron diffraction, these spectroscopic techniques provide a less direct approach for studying the ice structure, but the observed spectral variations can be related to changes in the optical and morphological ice properties. Molecular hydrogen can reside in porous CO ice at low temperatures near 10 K; the desorption of H_2 during warm-up of CO ice could thus be an indication of porosity. To test this possibility, a quadrupole mass spectrometer (QMS) was used to monitor the desorption of H_2 and CO molecules from solid CO deposited at 8 and 20 K. The information gathered from all our experiments could serve to trace the evolution of pure CO ice as a function of ambient or accretion temperature in dust grains present in dense cloud interiors. The data was used to test if re-structuring toward a more compact ice can explain the (here confirmed) decrease of the CO photodesorption yield for increasing deposition temperatures.

2. Experimental

The UV-irradiation of CO ice experiments, aiming to study the photodesorption rate as a function of deposition temperature, were perfomed using the InterStellar Astrochemistry Chamber (ISAC) at the Center of Astrobiology near Madrid, an ultra-high vacuum setup ($2.5-4.0 \times 10^{-11}$ mbar) where ice samples were made by depositing CO gas onto a KBr substrate window placed at the cold finger of a closed-cycle helium cryostat

at 7−20 K. Samples were UV-irradiated using a microwave-stimulated hydrogen flow discharge lamp (MDHL) that provides a flux of 2.5×10^{14} photons cm^{-2} s^{-1} at the sample position with an average photon energy of 8.6 eV. The characterization of the MDHL spectrum was previously reported (Cruz-Diaz et al. 2014) and was discussed in more detail by Chen et al. (2014). The VUV spectrum was measured routinely in situ during the experiments with the use of a McPherson 0.2 meter focal length VUV monochromator (Model 234/302) with a photomultiplier tube (PMT) detector that was equipped with a sodium salicylate window, optimized to operate from 100−500 nm (11.27−2.47 eV), with a spectral resolution of 0.4 nm. The VUV absorption spectrum of CO ice deposited at different temperatures was obtained as the difference of the cold substrate spectra before and after ice deposition. For more details on the experimental protocol employed for VUV spectroscopy, see Cruz-Diaz et al. (2014).

Temperature-programmed desorption experiments employed a constant heating ramp of 1 K min^{-1}. The ice was monitored by in situ transmittance Fourier transform infrared (FTIR) spectroscopy (Bruker VERTEX 70) at a spectral resolution of 1 cm^{-1}, while the volatile species were recorded with a quadrupole mass spectrometer (QMS) equipped with a Channeltron detector (Pfeiffer Vacuum, Prisma QMS 200). For an in depth description of ISAC, we refer to Muñoz Caro et al. (2010).

The column density of the deposited ice is calculated according to the formula

$$N = \frac{1}{A} \int_{\text{band}} \tau_\nu \, d\nu, \tag{1}$$

where N is the column density in cm^{-2}, τ_ν the optical depth of the band, $d\nu$ the wavenumber differential in cm^{-1}, and A the band strength in cm molecule^{-1}. The integrated absorbance is equal to $0.43 \times \tau$, where τ is the integrated optical depth of the band. The adopted band strength for CO was $A(CO) = 1.1 \times 10^{-17}$ cm molecule^{-1} (Jiang et al. 1975).

The infrared spectroscopy of CO ice deposited at different temperatures was performed using the Interstellar Photoprocess System (IPS) at the National Central University in Jhongli City (Taiwan). This setup and the experimental protocol are described in detail in Chen et al. (2014). Briefly, the IPS consists of an ultra-high-vacuum (UHV) chamber equipped with a closed-cycle helium cryostat, with a background pressure of $\sim 1 \times 10^{-10}$ torr. Ice films were deposited on a KBr window attached to the tip of a cold finger. The temperature of the KBr window was controlled by a tunable heater with a 0.1 K accuracy from 14 K to 400 K. The CO ice samples were monitored in situ using an FTIR spectrometer equipped with a mercury-cadmium-telluride (MCT) detector in the transmission mode. Infrared spectra were acquired with a 1 cm^{-1} resolution and averaged over 128 scans. The angle between the IR beam and the ice sample was 45°. Similar experiments with a 15° incidence angle, but a higher IR spectral resolution of 0.1 cm^{-1}, were performed at the Institute of Chemical Studies from Heriot-Watt University in Edinburgh, depositing CO onto a copper substrate coated with 300 nm SiO_2; a detailed description of these experiments is provided in Lasne et al. (2015).

While spectral resolution defines the ability to resolve bands of close proximity, the detection of a peak broadening or a peak shift is also related to the wavenumber accuracy of the instrument. FTIR allows for better accuracy of the wavenumber scale than dispersive spectrometers because every scan can be calibrated with a He/Ne laser which has a stable and accurately known wavelength (White 1990). The peak wavenumber

accuracy of the FT-IR instrument coupled to the IPS setup is <0.04 cm^{-1}, and the wavenumber repeatability is <0.002 cm^{-1}. Peak shifts can become observable even when the natural peak width is smaller than the instrument is capable of measuring (e.g., Spectral Resolution in FT-IR Spectroscopy, Application Note AN#71, Bruker Optics). According to this reference, it is possible to detect a peak shift smaller than the working resolution. In Sect. 3, the peak shift observed in Fig. 1 as a function of ice temperature reaches a maximum value of 0.6 cm^{-1}, i.e., lower than the 1 cm^{-1} working resolution. This peak shift is expected to be more pronounced at higher spectral resolution measurements using the same incidence angle (Spectral Resolution in FT-IR Spectroscopy, Application Note AN#71, Bruker Optics). The observed wavelength shifts were reproducible within small errors of 0.04 cm^{-1}, corresponding to the wavenumber accuracy. In addition, no shift was observed in a warm-up experiment of ice deposited at 14 K.

In the 0.1 cm^{-1} high resolution experiments performed at Heriot-Watt University, the errors in frequencies are ±0.01 and ±0.02 cm^{-1} for the modes near 2142 cm^{-1} and 2138 cm^{-1}, respectively. Similar to the National Central University, no shift was observed in an annealing experiment of ice deposited at 18 K and warmed up to 26 K. Finally, shifts were observed only for deposition temperatures above 20 K in both series of experiments, the 1 cm^{-1} and 0.1 cm^{-1} spectral resolution measurements using different incidence angles, 45° and 15°, respectively.

3. Infrared spectroscopy of CO ice

The presence of CO in astrophysical ices is generally inferred from the detection of an infrared absorption band near 2137 cm^{-1}, which is caused by the CO stretching vibration. The FWHM for pure CO ice deposited at 10 K is about 2.5 cm^{-1}. It decreases to 2.0 cm^{-1} after warming up to 30 K. Pure CO films deposited above 20 K present lower FWHM values of 1.0 to 1.5 cm^{-1} (Sandford et al. 1988, and references therein). Although a systematic study of the infrared spectroscopy of solid CO as a function of deposition temperature was not found in the literature, a compilation of several works provides an estimate of the optical constants at 10, 12, 12.5, 16, and 20 K: the real n values of the refractive index are about 2.656, 2.457, 2.225, 2.948, and 1.432, while the imaginary part k values are rounded to 1.255, 0.984, 0.447, 1.055, and 0.086 (Roux et al. 1979; Hudgins et al. 1993; Baratta & Palumbo 1998; Elsila et al. 1997; Palumbo et al. 2006). With the exception of the relatively low value measured at 20 K, the oscillations of these values are likely due to experimental variations within the different laboratory conditions and protocols. The longitudinal (LO) and transverse (TO) optical modes of solid CO near 2142 and 2138 cm^{-1}, respectively, were reported by, for example, Palumbo et al. (2006). Most works dedicated to IR spectroscopy of ices use unpolarized light at normal incidence angle where only the TO mode is observed. In our IR measurements, using unpolarized light with a 45 or 15° incidence angle, both the LO and TO modes are observable, although the expected intensity of the LO band is low compared to p-polarized IR beam measurements. This was confirmed in the experiments reported below. While the LO-TO splitting is readily understood in the case of crystalline solids, we observe that the LO and TO bands are also observed in CO ice deposited at 14 K, which is expected to be amorphous. The infrared spectrum of solid CO, and in particular the LO-TO splitting, depends on dipole-dipole interactions alone, and short-range interactions add a weak broadening (Zumofen 1978).

The top panel of Fig. 1 displays the spectra collected at different CO ice deposition temperatures with a spectral resolution of 1 cm^{-1} and a 45° incidence angle. The column density of all the samples was similar, between 5.4–6.1×10^{16} molecules cm^{-2}. The bottom panel of Fig. 1 represents the central peak positions of the CO bands, calculated using a two-Gaussian deconvolution, while matching the resolution of the real data, for: the warm-up experiment of ice deposited at 14 K at the National Central University, the deposition experiments performed at different temperatures with a spectral resolution of 1 cm^{-1} and a 45° incidence angle, and similar deposition experiments with a high spectral resolution of 0.1 cm^{-1} and a small incidence angle of 15°. The experiments performed at high resolution used an estimated ice column density of about 5×10^{15} molecules cm^{-2}.

There is a clear shift in the band positions for CO deposition temperatures above 20 K in the low- and high-resolution experiments, which was not observed in the warm-up experiment. In the 20 to 26 K deposition temperature range, the TO band near 2138 cm^{-1} is blue-shifted by 0.13 cm^{-1} in the high resolution experiment, while the LO band near 2142 cm^{-1} is red-shifted by 0.14 cm^{-1}, and the LO-TO splitting therefore varies from 4.02 cm^{-1} at 20 K to 3.75 cm^{-1} at 26 K (LO-TO splitting decreases about 0.27 cm^{-1}), as reported in Lasne et al. (2015). These shifts are more pronounced in the low-resolution experiments: in the same temperature range the TO and LO bands shifts are about 0.3 and 0.6 cm^{-1}, respectively, and the corresponding LO-TO splitting diminishes from about 4.4 cm^{-1} at 20 K to 3.5 cm^{-1} at 26 K (LO-TO splitting decreases about 0.9 cm^{-1}, i.e., by a factor of 3.3 larger than in the high resolution experiment). Since the LO-TO splitting does not seem to depend on the incidence angle (e.g., Zumofen 1978), the amplitude of this effect is attributed to the different resolutions used in both experiments, as mentioned in Sect. 2, but the shift trends are in the same direction. It should be noted that, first, a proper study of this effect, which is beyond the scope of our paper, would require high-resolution measurements of 0.1 cm^{-1} in the 45° experiments (as it was done for the 15° measurements), and second, the CO samples deposited in our experiments differ from a crystal and, consequently, the origin of the LO-TO splitting is not obvious, as mentioned above, the incident infrared beam impinges on the CO dipole molecules at various angles, even when the incidence angle with respect to the substrate is fixed at 15° or 45°.

With the exception of the substrate temperature during ice deposition, the experimental parameters were the same for the experiments in each series: the same substrate window for the deposition, the same deposition time and CO gas pressure increment (ΔP) during deposition leading to a similar ice thickness, and the same incidence angle. This observation led us to conclude that the tiny, yet clear and reproducible, shifts in the LO and TO bands as a function of CO ice-deposition temperature, starting at about 20 K, are due to a different morphology of the ice deposited at the higher temperatures, as is commonly reported for other ices in the literature. We note that the warm-up experiments, where CO ice was grown at 14 K or 18 K, and then gradually warmed up at 1 K min^{-1}, did not lead to a shift in these bands: the spectrum remained unaltered during warming up to 26 K. Therefore, a different ice morphology is associated with the ice deposition temperature, while the temperature achieved during warming up to 26 K did not change the optical constants of the ice in our experiments. Similar spectroscopic studies are documented for other pure ices, but unlike CO, other molecular solids like H_2O, H_2S, or CO_2 ice display clear variations in
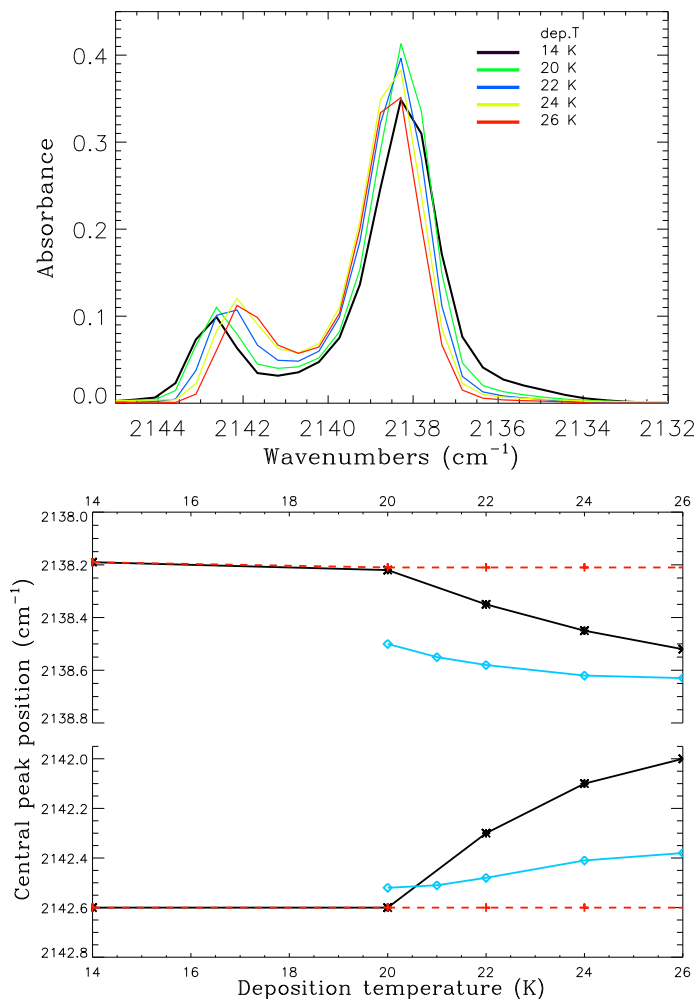
Fig. 1. *Top*: spectra collected at different CO ice deposition temperatures with a spectral resolution of 1 cm^{-1} and a 45° incidence angle. *Bottom*: central peak positions of the CO bands corresponding to warm-up of ice deposited at 14 K, spectral resolution of 1 cm^{-1} and 45° incidence angle (crosses, red trace), the deposition experiments performed at different temperatures with a spectral resolution of 1 cm^{-1} and 45° incidence angle (asterisks, black trace), and deposition experiments at different temperatures with high spectral resolution of 0.1 cm^{-1} and 15° incidence angle (diamonds, blue trace). The observed frequency shifts were reproducible within small errors of 0.04 cm^{-1}, corresponding to the wavenumber accuracy, in the low-resolution experiments. Frequency shifts in the high-resolution experiments reported in Lasne et al. (2015) are ±0.01 and ±0.02 cm^{-1} for the LO and TO modes, respectively.

the IR band profiles during warm-up (e.g., Hagen et al. 1983; Jiménez-Escobar et al. 2011; Escribano et al. 2013).

4. Vacuum-ultraviolet spectroscopy of CO ice

Vacuum-ultraviolet spectroscopy is related to the electronic structure of the molecules in the ice, which could be altered by changes in the ice morphology during, for example, phase transition from an amorphous to a crystalline ice. There are very few studies dedicated to the VUV spectroscopy of solid CO (Brith & Schnepp 1965; Lu et al. 2005; Mason et al. 2006; Cruz-Diaz et al. 2014). The series of bands observed between 120 and 160 nm is attributed to the A^1 Π ← X^1 Σ$^+$ system. Lu et al. (2005) suggest that for these bands the electronic excitation seems to be largely localized within individual molecules, although according to these authors, the slight variation in the

vibrational coefficients for different conditions in the solid phase indicates a significant perturbing influence of the environment. In particular, no systematic work was found in the literature to study the effect of ice deposition temperature on the VUV spectral features. The CO ice deposition temperature of earlier works by Cruz-Diaz et al. (2014), Lu et al. (2005), Brith & Schnepp (1965), and Mason et al. (2006), was 8 K, 10 K, 20 K, and 26 K, respectively. For this reason, we conducted a series of experiments where CO ice was deposited at temperatures ranging from 8 K to 26 K and the VUV spectra were recorded. The CO ice column density in these experiments was about 5.0×10^{16} molecules cm^{-2}. The top panel of Fig. 2 displays the collected VUV spectra between 115 and 180 nm. A redshift is observed following the increase in CO ice deposition temperature. A similar shift becomes apparent after a comparison of the literature spectra collected at four different temperatures, see above references. This redshift is more pronounced at longer wavelengths. The previously reported Davydov splitting of the CO lines (Brith & Schnepp 1965) also affects the absorption band profiles and was found to vary with the ice deposition temperature in our experiments. This effect, which is related to the interaction of two non-translationally equivalent molecules, depends on the angle of the transition dipole moments and the distance between the molecules (De Rossi et al. 1996, and references therein). Therefore, the (0, 0) line centered near 156.6 nm is less affected by Davydov splitting and displays the most pronounced redshift, see middle panel of Fig. 2; for these reasons, this line was selected to represent the redshift as a function of CO ice deposition temperature in the bottom panel of Fig. 2. No shift is observed for deposition temperatures below 20 K. Above 20 K, the redshift in wavelength is noticeable and increases with deposition temperature. The deposition temperature of 26 K is close to thermal desorption of the CO ice; at this temperature the (0, 0) peak position is displaced by about 1 nm compared to the deposition temperatures below 20 K. Although the reason for this redshift in wavelength is not understood, it might be related to the physical structure of the CO ice as CO changes from amorphous to crystalline, since this transition affects the molecular environment and, consequently, the observed band system, as proposed by Lu et al. (2005). Indeed, the largest shift in the (0, 0) band is observed between CO gas, centered at 154.4 nm according to Lee & Guest (1981), and the ice deposited at 26 K is expected to be crystalline, centered at 157.6 nm. From this perspective, the appearance of the redshift around 20 K suggests that a modification in the physical structure of CO ice starts at this deposition temperature and increases gradually at higher deposition temperatures.

5. Thermal desorption of CO ice

Temperature programmed desorption (TPD) experiments of pure CO ice using the ISAC set-up, with a heating ramp of 1 K min^{-1}, were reported in Muñoz Caro et al. (2010). In UHV chambers with steel walls like ISAC, H$_2$ is a contaminant observed in the residual gas by mass spectrometry. It was found that a good fit of the TPD curve of CO deposited at 7 K, using the Polanyi-Wigner equation of exponential type, required a second exponential term. This contribution was associated with the release of H$_2$ trapped in CO ice, which ejects a small fraction of the CO molecules, see Fig. 3. This figure also includes the TPD curve of an experiment where CO was deposited at 20 K, and then cooled down to 7 K before warm-up, where contribution from H$_2$ is not observed. The 20 K deposition experiment was recently repeated with a slower heating ramp of 0.2 K min^{-1},
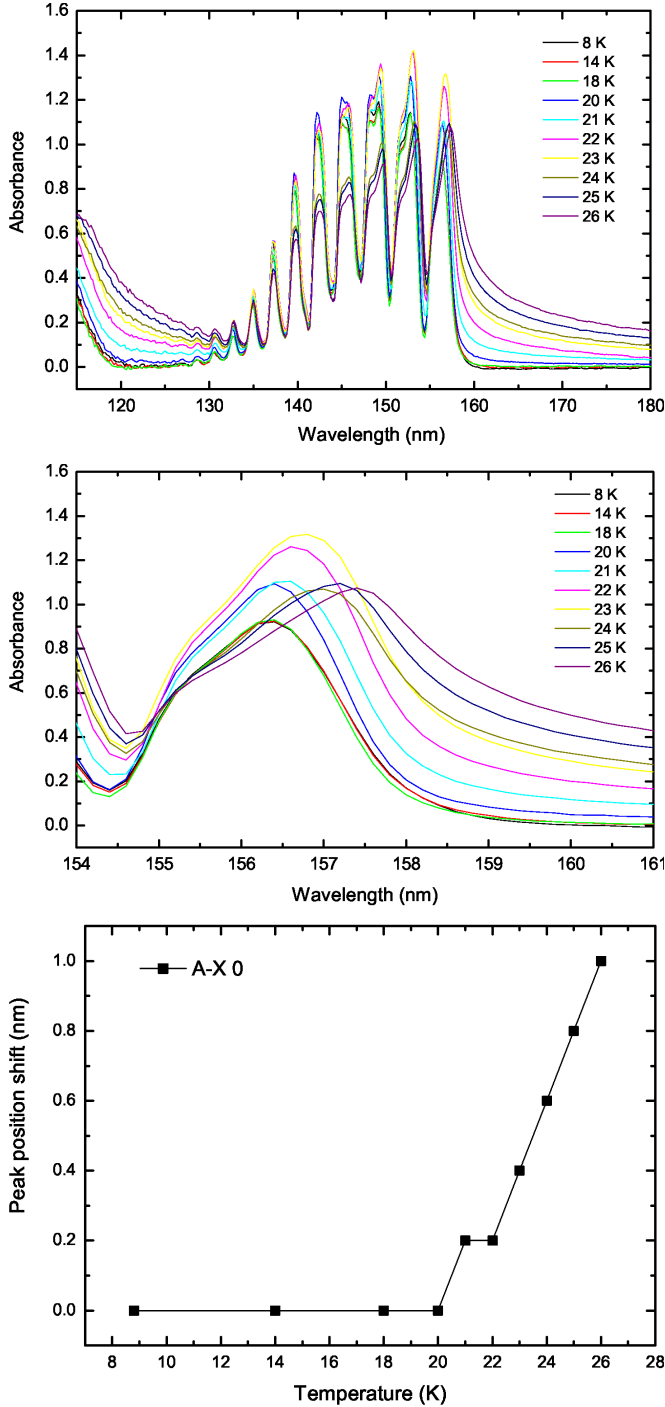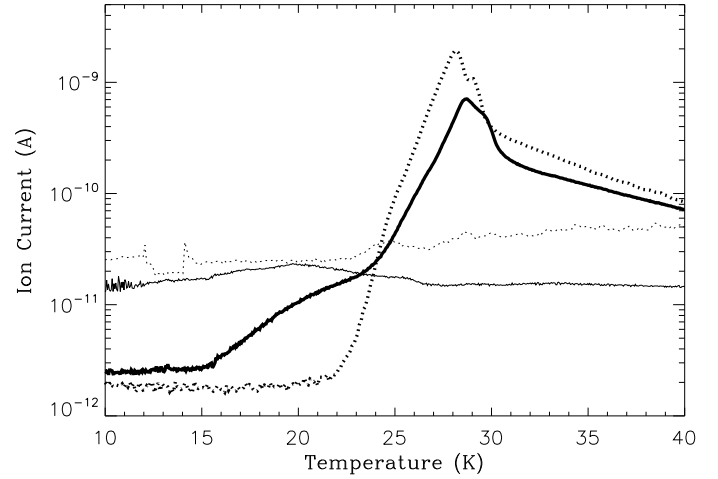
Fig. 3. CO ice desorption during warmup at a rate of 1 K min⁻¹ for sample deposited at 7 K (thick solid trace) and sample deposited at 20 K and cooled down to 7 K before warming up (thick dotted trace). The desorptions of H_2 in the samples deposited at 7 K (thin solid trace) and 20 K (thin dotted trace) are also shown (adapted from Muñoz Caro et al. 2010). The ion current (A) is plotted in a logarithmic scale for a better appreciation of the curve profile and corresponds roughly to partial pressure in mbar.

6. Photodesorption of CO ice

The CO ice irradiation temperature does not affect the photodesorption yield, only the temperature of CO ice deposition plays a role in the photodesorption, since the photodesorption yield was inversely proportional to the deposition temperature in the 15−27 K range (Öberg et al. 2009).

Figure 4 represents the decrease of the CO ice IR absorption as a function of UV fluence for two ice samples deposited at 8 K and 20 K using the ISAC set-up. The CO ice column density, obtained from Eq. (1), is often expressed as the number x of ice monolayers (ML), where 1 ML is defined as 1×10^{15} molecules cm⁻² and, therefore, $N = x \times 10^{15}$ molecules cm⁻². We note that the decrease of the CO ice column density is mainly driven by photodesorption of CO molecules, since no more than 5% of the UV photons absorbed in the ice leads to product formation in these experiments (Muñoz Caro et al. 2010). In the 8 K and 20 K experiments, the decrease of the CO ice column density is linear with fluence until about 5 ML of ice are left on the substrate, i.e., the photodesorption yield is constant in this regime, in line with previous works (Muñoz Caro et al. 2010; Fayolle et al. 2011; Chen et al. 2014). The photodesorption decreases exponentially for x below 5 ML. The following equations provide a fit of the consecutive data points in Fig. 4:

$$N(i) = N(i-1) - R_{\text{ph-des}}(x < 5\text{ML})(i-1) \cdot (t(i) - t(i-1)), \quad (2)$$

where t is the irradiation time and $R_{\text{ph-des}}(x < 5\text{ML})$ is the photodesorption rate in molecules cm⁻² s⁻¹, which depends on the number of photons absorbed as a function of the decreasing ice column density N during irradiation, and

$$R_{\text{ph-des}}(x < 5\text{ML}) = I_0 \cdot (1 - k \cdot e^{-\sigma N}) \cdot QY, \quad (3)$$

where $I_0 = 2.5 \times 10^{14}$ photons cm⁻² s⁻¹ is the UV flux at the sample position. We adopted a UV absorption cross-section of $\sigma = 4.7 \times 10^{-18}$ cm² for the average photon energy (8.6 eV) of our UV lamp; this energy falls within the absorbing spectral
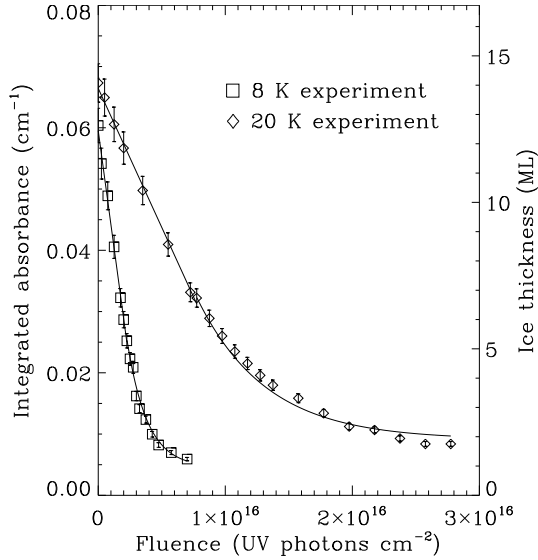
Fig. 2. *Top*: VUV spectra between 115 and 180 nm corresponding to different deposition temperatures between 8.8 and 26 K. *Middle*: zoom of the (0, 0) band near 156.6 nm showing a pronounced redshift. *Bottom*: representation of the (0, 0) band wavelength shift as a function of ice-deposition temperature.

allowing H_2 more time to enter the CO ice, data not shown, but the result was similar: no desorption of H_2 was observed. These results indicate that CO ice deposition at 7 K allows trapping of H_2 while deposition at 20 K does not. The CO ice formed at 20 K and then cooled down to 7 K does not contain H_2 (since no H_2 desorbs during warm-up of this ice), because H_2 is not capable of entering the already formed compact ice, meaning that H_2 would only physisorb during ice deposition at 7 K.

Fig. 4. Decrease in the CO ice absorption in the IR as a function of UV fluence for two ice samples deposited at 8 K (squares) and 20 K (diamonds). Solid lines are the fits, see text for an explanation.
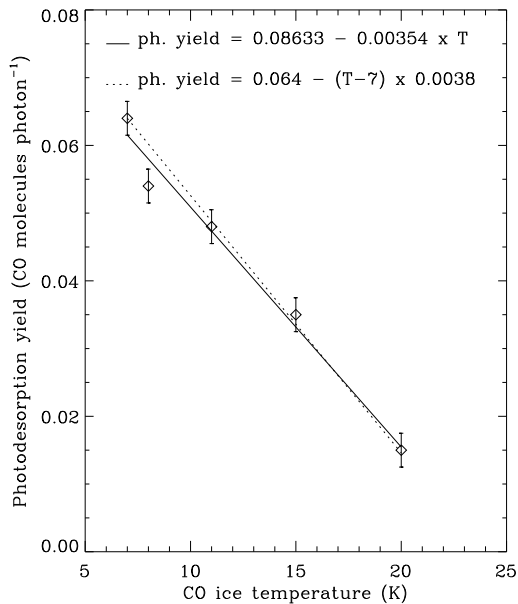

Fig. 5. Photodesorption yield, in molecules per incident photon in the ice as a function of CO ice-deposition temperature. The solid line is the best linear fit of the data points, the dotted line is an alternative fit.

7. Astrophysical implications and conclusions

The morphology of ice mantles was extensively discussed in the literature. The ice observed toward young stellar objects (YSOs) and dense interstellar cloud interiors is often built up with several components, distributed in a mixed or a segregated multilayered ice mantle configuration. It was proposed that the fit of the observed solid CO infrared band requires a three phase model, where CO is present in a i) weakly polar environment, like pure CO; ii) CO mixed with other weakly polar or apolar species, such as CO_2, N_2 or O_2; and iii) CO mixed with polar species like methanol. The middle component of the CO band near 2139.7 cm^{-1}, corresponding to pure CO (e.g., Pontoppidan et al. 2003; Penteado et al. 2015), could present different degrees of amorphicity toward a crystalline ice structure, depending on the formation temperature of the CO ice that covers dust grains.

Water ice deposited at different temperatures is known to display important peak position and shape variations that allow a more straightforward determination of its thermal history in icy grain mantles (Hagen et al. 1983). On the other hand, infrared observations require a very high spectral resolution, about 0.1 cm^{-1}, to accurately estimate the position of the CO absorption that peaks near 2140 cm^{-1}, and to estimate its accretion temperature. The infrared spectroscopy of solid CO ice analogs reported in this work can be used for this purpose. Indeed, given the small shift of ~0.6 cm^{-1} for CO ice deposition at $T = 26$ K, compared to $T \leq 20$ K, these observations are technically challenging. Other potential sources of small deviations, less than 1 cm^{-1}, from the band position of CO formed at temperatures near 10 K could be i) mixing with apolar species or ii) the effects of grain size/shape.

The ice deposition temperature of CO has a strong effect in the photodesorption rate, see Fig. 5. It is thus appropriate to discuss how the configuration of the CO molecules in the solid can vary as a function of deposition temperature. The surface charging measured in condensates (ices) of gases with a dipole moment, in particular CO, was found to be the result of polarization, i.e., the ordering of the dipole molecules during deposition (Kutzner 1972). A dependence of the polarization on the deposition temperature was explained by a resonance mechanism between the oscillation frequency of the accommodating molecules and the mean phonon frequency of the substrate material or the deposited ice layer, respectively. This work provided a clear description of the condensation process as a function of the substrate temperature, which we summarize hereafter. The CO molecules strike the substrate with an energy of rotation and translation according to room temperature. The accommodation takes place within a time of 10^{-10} to 10^{-11} s. During that time the spare energy has to be stored up in different degrees of freedom. One possibility of movement for a CO molecule on the surface is that of pendulum oscillations that occur if one end of the molecule (e.g., carbon) is fixed to the substrate and the other end (e.g., oxygen) can oscillate freely. The potential V of these oscillations is equal for both possible orientations, whereas the moment of inertia I depends on the mass of the oscillating atom. Therefore the eigenfrequencies ω_O and ω_C of the oxygen and carbon oscillations, respectively, are determined by the orientation of the molecule and are given by:

$$\omega_O = \sqrt{\frac{V}{I}} = \sqrt{\frac{V}{r^2 m_O}}; \omega_C = \sqrt{\frac{V}{r^2 m_C}}. \qquad (4)$$

If there is resonance between the mean phonon frequency of the substrate, or the already deposited ice layer, and one of the oscillation frequencies of the accommodating CO molecule, with

region of CO ice (Cruz-Diaz et al. 2014). The quantum yield values, QY, at 8 and 20 K are, respectively, 2.24, and 0.655 desorbing molecules per absorbed photon in the top 5 ML. The dimensionless k parameter values used to fit the data points in Fig. 4 for the 8 and 20 K experiments are 1.0045 and 1.009, respectively. We refer to Muñoz Caro et al. (2010) for more details on the fit equations.

Figure 5 displays the photodesorption yield values with estimated error bars, in molecules per incident photon for $x \geq 5$ ML, measured in several irradiation experiments where the CO ice samples were deposited at different temperatures of 7, 8, 11, 15, and 20 K, respectively. The linear equation that provides the best fit for the photodesorption yield as a function of CO ice deposition temperature T is included in this figure (solid line), while the dotted line is an alternative fit.

oxygen at the free oscillating end for instance, then the energy transfer to the condensate is detained for this orientation. The not yet completely accommodated molecules can move on the surface and turn over from one orientation to the other. Therefore, finally, more molecules will be condensed in the non-detained orientation. At low temperatures the dependence of the phonon distribution on temperature and frequency can be described by Debye's approximation. At these temperatures the mean phonon frequency is proportional to the absolute temperature. It is remarkable that the sticking probability, referred to as the capture coefficient in Dawson & Haygood (1965), does not vary as a function of ice surface temperature between 10 and 25 K; these authors report a value of $0.85-0.90$ with a 5% accuracy for a gas temperature of 300 K, which agrees with the value of 0.87 ± 0.05, as estimated at 14 K by Bisschop et al. (2006).

We showed that monitoring of solid CO that was deposited at various deposition temperatures by IR and VUV spectroscopy observed band shifts only above 20 K. This variation is close to the transition temperature from amorphous to crystalline ice near 23 K reported by Kouchi (1990) using electron diffraction. The spontelectric effect, i.e., the generation of a spontaneous electric field in ices composed of dipole molecules, was recently reported for solid CO, and the shift of the IR bands above 20 K was related to this electric field (Lasne et al. 2015). The density and refractive index n recently measured by Satorre et al. (in prep.), follow the trend that we observed spectroscopically in the IR and UV ranges, i.e., the change to a more compact configuration (higher ice density) only occurs above 20 K. The gradual and linear decrease in the photodesorption yield as the CO ice deposition temperature increases from 7 K to 20 K can, therefore, not be explained by variations in the ice morphology toward a crystalline ice. A different explanation is needed.

The photodesorption of pure CO occurs via the desorption induced electronic transition (DIET) mechanism, by which the photon energy must be transferred from the first excited molecule to the desorbing molecule on the ice surface. It seems reasonable to think that the value of the photodesorption rate will depend on the efficiency of photon energy transfer between molecules. The recent publication of Romanova et al. (2014) offers evidence of a strong dependence of energy transfer on the CO ice deposition temperature as a consequence of disorder in the glassy state. In this work, the thermal conductivity of the solid grown in an ampoule was measured. The maximum in thermal conductivity was already observed at 3 K and dropped from ~10 to ~1 W m^{-1} K^{-1} in the 7 to 20 K deposition temperature range.

The onset of CO ice formation in cold inter- and circumstellar environments is expected at temperatures near 20 K. According to Fig. 5, the corresponding photodesorption yield is a factor of about 4 lower, compared to ice deposition at 7 K. Dust models that incorporate photodesorption of CO and other species should therefore adopt yield values that are compatible with the thermal history of the cloud. Although the propagation of photon energy via the DIET mechanism fundamentally differs from thermal energy transfer in the solid, the strong dependence with ice deposition temperature of both the thermal conductivity (Romanova et al. 2014, and references therein) and the photodesorption rate, suggests that, as is the case of thermal conductivity, the photodesorption of CO is influenced by the degree of disorder of CO dipoles in the amorphous or glassy state. We emphasize that this effect of dipole disorder in the photodesorption, which occurs at deposition temperatures in the 7 K to 20 K range, is not directly related to the transition from amorphous to crystalline solid CO, which is triggered at temperatures above 20 K.

References

Acharyya, K., Fuchs, G. W., Fraser, H. J., van Dishoeck, E. F., & Linnartz, H. 2007, A&A, 466, 1005

Baratta, G. A., & Palumbo, M. E. 1998, J. Opt. Soc. Amer. A., 15, 3076

Bertin, M., Fayolle, E. C., Romanzin, C., et al. 2012, Phys. Chem. Chem. Phys., 14, 9929

Bertin, M., Fayolle, E. C., Romanzin, C., et al. 2013, ApJ, 779, 120

Bisschop, S. E., Fraser, H. J., Öberg, K. I., van Dishoeck, E. F., & Schlemmer, S. 2006, A&A, 449, 1297

Brith, M., & Schnepp, O. 1965, Mol. Phys., 9, 473

Chen, Y.-J., Chuang, K.-J., Muñoz Caro, G. M., et al. 2014, ApJ, 781, 15

Collings, M. P., Anderson, M. A., Chem, R., et al. 2004, MNRAS, 354, 1133

Cruz-Diaz, G. A., Muñoz Caro, G. M., Chen, Y.-J., & Yih, T.-S. 2014, A&A, 562, A119

Dartois, E. 2006, A&A, 445, 959

Dawson, J. P., & Haygood, J. D. 1965, Cryogenics, 5, 57

De Rossi, U., Dähne, S., Meskers, S. C. J., & Dekkers, H. P. J. M. 1996, Angew. Chem. Int. Ed. Engl., 35, 760

Elsila, J., Allamandola, L. J., & Sandford, S. A. 1997, ApJ, 479, 818

Escribano, R. M., Muñoz Caro, G. M., Cruz-Diaz, G. A., Rodríguez-Lazcano, Y., & Mate, B. 2013, PNAS, 110, 12899

Fayolle, E. C., Bertin, M., Romanzin, C., et al. 2011, ApJ, 739, L36

Gerakines, P. A., Schutte, W. A., & Ehrenfreund, P. 1996, A&A, 312, 289

Hagen, W., Tielens, A. G. G. M., & Greenberg, J. M. 1983, A&SS, 51, 389

Hudgins, D. M., Sandford, S. A., Allamandola, L. J., & Tielens, A. G. G. M. 1993, ApJS, 86, 713

Jiang, G. J., Person, W. B., & Brown, K. G. 1975, J. Chem. Phys., 64, 1201

Jiménez-Escobar, A., & Muñoz Caro, G. M. 2011, A&A, 536, A91

Kouchi, A. 1990, J. Cryst. Growth, 99, 1220

Kutzner, K. 1972, Thin Solid Films, 14, 49

Lasne, J., Rosu-Finsen, A., Cassidy, A., McCoustra, M. R. S., & Field, D. 2015, Phys. Chem. Chem. Phys., 17, 30177

Lee, L. C., & Guest, J. A. 1981, J. Phys. B: At. Mol. Phys., 14, 3415

Loeffler, M. J., Baratta, G. A., Palumbo, M. E., Strazzulla, G., & Baragiola, R. A. 2005, A&A, 435, 587

Lu, H.-C., Chen, H.-K., Cheng, B.-M., et al. 2005, J. Phys. B: At. Mol. Opt. Phys., 38, 3693

Martín-Doménech, R., Manzano-Santamaría, J., Muñoz Caro, G. M., et al. 2015, A&A, 584, A14

Mason, N., J., Dawes, A., Holtom, P. D., et al. 2006, Faraday Discussions, 133, 311

Muñoz Caro, G. M., Jiménez-Escobar, A., Martín-Gago, J. Á., et al. 2010, A&A, 522, A108

Öberg, K. I., Fuchs, G. W., Awad, Z., et al. 2007, ApJ, 662, L23

Öberg, K. I., van Dishoeck, E. F., & Linnartz, H. 2009, A&A, 496, 281

Palumbo, M. E., & Strazzulla, G. 1993, A&A, 269, 568

Palumbo, M. E., Baratta, G. A., Collings, M. P., & McCoustra, M. R. S. 2006, Phys. Chem. Chem. Phys. 8, 279

Penteado, E. M., Boogert, A. C. A., Pontoppidan, K. M., et al. 2015, MNRAS, 454, 531

Pontoppidan, K., M., Fraser, H. J., Dartois, E., et al. 2003, A&A, 408, 981

Romanova, T., Stachoviak, P., & Jeżowski, A. 2014, Solid State Communications, 197, 6

Roux, J. A., Wood, B. E., Smith, A. M., & Plyler, R. R. 1979, Tech. Rep. Arnold Air Force Stat. AEDC-TR-79-81 (Arnold Air Force Base: AEDC)

Sandford, S. A., & Allamandola, L. J. 1988, Icarus, 76, 201

Sandford, S. A., Allamandola, L. J., Tielens, A. G. G. M., & Valero, G. J. 1988, ApJ, 329, 498

van Hemert, M. C., Takahashi, J., & van Dishoeck, E. F. 2015, J. Phys. Chem A, 119, 6354

White, R. 1990, Chromatography/Fourier transform infrared spectroscopy and its applications (New York: Marcel Dekker, Inc.)

Zumofen, G. 1978, J. Chem. Phys., 68, 3747